DOI 10.24425/aee.2023.147428

# Simulation study on the structural optimization of composite insulators based on contaminant deposition

YUKUN LV, ZEZE CHEN ✉, QIAN WANG, YAO LU, XIAOJING LI

*Department of Power Engineering, School of Energy, Power and Mechanics*
*North China Electric Power University, China*
*e-mail:* ✉*17854201242@163.com*

(Received: 30.05.2023, revised: 25.09.2023)

**Abstract:** Optimizing the aerodynamic structure of composite insulators can guarantee the safe operation of power systems. In this study, we construct a simulation model for composite insulator contaminant deposition using the COMSOL simulation software, and the rationality of the simulation model and method is verified through wind tunnel experiments. Taking the FXBW4-110/100 composite insulator as an example, we adopt a progressive optimization plan to explore the impacts of shed spacing $s$, and shed inclination angles $\alpha$ and $\beta$ on its contaminant deposition characteristics under DC and AC voltages. Based on the numerical simulation results, we analyze the antifouling performance of insulators before and after structural optimization. The results indicate the following: 1) The contaminant deposition of the insulator under AC and DC voltages is negatively correlated with the shed spacing $s$, but positively correlated with the lower inclination angle $\beta$. 2) Under AC voltages, the contaminant deposition of the insulator increases with the upper inclination angle $\alpha$, while under DC voltages, the contaminant deposition shows an uptrend first, then a downtrend and then an uptrend again with the increase of the upper inclination angle $\alpha$. 3) Compared with the original model, the AC-optimized model ($\alpha = 6°$, $\beta = 2°$ and $s = 98$ mm) with a larger shed spacing $s$, and smaller shed inclination angles $\alpha$ and $\beta$ showed superior antifouling performance at wind speeds of no less than 2 m/s, and under the typical conditions ($v = 2.5$ m/s, $d = 20$ μm, and $\rho = 2\,200$ kg/m$^3$), its contaminant deposition is 15% less than that of the original model ($\alpha = 10°$, $\beta = 2°$ and $s = 80$ mm).

**Key words:** composite insulator, contaminant deposition characteristics, numerical simulation, voltage type, structural optimization

## 1. Introduction

Composite insulators (hereinafter referred to as "insulators"), which are commonly used in power systems, are crucial insulation devices with a typical aerodynamic structure [1]. If conductive particles settle on the surface of an insulator, its dielectric properties would be affected, potentially resulting in the formation of a continuous conductive layer on the surface, which may cause a contamination flashover accident, particularly in humid weather, leading to significant financial losses [2, 3]. Optimizing the aerodynamic structure of insulators can help reduce the amount of surface contaminant deposition, which is essential for ensuring the safe operation of transmission lines.

In recent years, numerous studies have been conducted to optimize insulator structures. Literature [4] studies impacts of insulator shed shape on anti-aging performance in salt-fog environments, and the study points out that an alternating diameter shed design is better than an equal-diameter shed design. Literature [5] conducts a study on shed materials of insulators, and the results indicate that compared to a shed made of pure silicone rubber, adding $TiO_2$ to the shed material formula can improve the shed's corrosion resistance and reduce insulator contaminant deposition. Literature [6] studies the impacts of the shed overhang and spacing on partial discharge among insulator sheds. It indicates that with the increase of the shed overhang, partial discharge becomes more intense, and the phenomenon of arc bridge connection between shed skirts becomes more prominent but weakens with the increase of the shed spacing. Literature [7] compares the contaminant deposition characteristics of insulators with different shed spacings through wind tunnel experiments and concludes that increasing the shed spacing can reduce surface contaminant deposition. Literature [8] investigates the flashover characteristics of insulators with various shed skirt structures through artificial contaminant deposition, icing and rain tests, and recommends the use of a shed structure that alternates between a large shed and a small shed or one large shed and two small sheds, provided that the creeping distance is met. Literature [9] designs an insulator with a nozzle structure and observes that the nozzle structure can effectively reduce the formation of the low-speed vortex region between the sheds of the insulator. Literature [10] investigates impacts of anti-flashover coatings on the flashover voltage of insulators and indicates that insulators coated with anti-flashover coatings show an increase in flashover voltage of approximately 25%. Literature [11] explores impacts of insulator shed diameter, shed spacing and metallic end fitting diameter on electric field distribution, and the results show that optimizing the structure of an insulator can improve the electric field distribution on the surface of the insulator and reduce its maximum electric field intensity.

Despite the rich research findings in the above studies, insulators typically operate under complex conditions such as contaminant deposition and raining. Furthermore, most studies on the structural optimization of insulators under contamination conditions use experimental methods, which may be constrained by poor economy, long periods. By contrast, the numerical simulation method has benefits such as low cost, short time and easy acquisition of single-factor impacts. Therefore, for the shortcomings of existing studies on the structural optimization of insulators under contamination conditions, this paper plans to use COMSOL to establish a simulation model of insulator contaminant deposition and verify the rationality of the simulation model and method through wind tunnel experiments. This paper takes the FXBW4-110/100 insulator as an example, and explores the impacts of shed inclination angles $\alpha$ and $\beta$, and shed spacing $s$ on

the contaminant deposition characteristics of insulators under DC and AC voltages. Based on the numerical simulation results, this paper optimizes structures of existing insulators in hopes of providing reliable guidance for insulator contamination prevention.

## 2. Simulation model for composite insulator contaminant deposition

### 2.1. Mathematical model and governing equations

#### 2.1.1. Flow field governing equation

When airflow passes around an insulator, the streamline experiences significant bending and turbulence anisotropy. To obtain simulation results that are closer to the actual results, the flow field uses the Reynolds time-averaged Navier-Stokes (RANS) method. For this reason, the NANS $k-\varepsilon$ model that can better handle high strain rates and large flow streamline bending during simulation is chosen. The governing equation for the flow field is shown in Formula (1) [12]:

$$\begin{cases} \rho(\boldsymbol{U}\cdot\nabla)\boldsymbol{U} = \nabla\cdot\left[-p\boldsymbol{I} + (\mu+\mu_{\mathrm{T}})\left(\nabla\boldsymbol{U} + (\nabla\boldsymbol{U})^{\mathrm{T}}\right) - \dfrac{2}{3}\rho k\boldsymbol{I}\right] + \boldsymbol{F} \\ \nabla\cdot\boldsymbol{U} = 0 \\ \rho(\boldsymbol{U}\cdot\nabla)k = \nabla\cdot\left[\left(\mu + \dfrac{\mu_{\mathrm{T}}}{\sigma_{\mathrm{k}}}\right)\nabla k\right] + p_{\mathrm{k}} - \rho\varepsilon \\ \rho(\boldsymbol{U}\cdot\nabla)\varepsilon = \nabla\cdot\left[\left(\mu + \dfrac{\mu_{\mathrm{T}}}{\sigma_{\varepsilon}}\right)\nabla\varepsilon\right] + C_{\varepsilon 1}\dfrac{\varepsilon}{k}p_{\mathrm{k}} - C_{\varepsilon 2}\rho\dfrac{\varepsilon^2}{k} \\ \mu_{\mathrm{T}} = \rho C_{\mu}\dfrac{k^2}{\varepsilon} \\ p_{\mathrm{k}} = \mu_{\mathrm{T}}\left[\nabla\boldsymbol{U} : \left(\nabla\boldsymbol{U} + (\nabla\boldsymbol{U})^{\mathrm{T}}\right)\right] \end{cases}, \tag{1}$$

where: $\boldsymbol{U}$ is the flow field velocity, in m/s; $\boldsymbol{I}$ is the main stress tensor, in Pa; $\mu$ and $\mu_{\mathrm{T}}$ are the air dynamic viscosity and turbulent dynamic viscosity, respectively, in Pa·s; $\rho$ is the air density, in $\mathrm{kg}^3$; $\boldsymbol{F}$ is the volume force, in $\mathrm{N/m}^3$; $k$is the turbulent kinetic energy, in $\mathrm{m}^2/\mathrm{s}^2$; $\varepsilon$ is the turbulent dissipation rate, in $\mathrm{m}^2/\mathrm{s}^3$; $C_{\mu}$ is the viscosity coefficient; $\sigma_{\mathrm{k}}$, $\sigma_{\varepsilon}$, $C_{\varepsilon 1}$, and $C_{\varepsilon 2}$ are turbulence model parameters; $p_{\mathrm{k}}$ is the energy source term of turbulence, in $\mathrm{W/m}^3$.

#### 2.1.2. Electric field governing equation

The electric field governing equation under DC voltages is shown in Formula (2) [13]:

$$\begin{cases} \nabla\cdot\boldsymbol{D} = \rho_v \\ \boldsymbol{E} = -\nabla V \\ \boldsymbol{D} = \varepsilon_0\varepsilon_{\mathrm{r}}\boldsymbol{E} \end{cases}, \tag{2}$$

where: $\boldsymbol{E}$ is the spatial electric field intensity, in V/m; $\boldsymbol{D}$ is the electric displacement intensity, in $\mathrm{C/m}^2$; $V$ is the electric potential, in V; $\varepsilon_{\mathrm{r}}$ is the relative permittivity of the material; $\varepsilon_0$ is the vacuum permittivity, being $8.8541878\times10^{-12}$ F/m; $\rho_v$ is the volume charge density, in $\mathrm{C/m}^3$.

The electric field governing equation under AC voltages is shown in Formula (3) [14]:

$$\begin{cases} \nabla \cdot \boldsymbol{J} = Q_{\mathrm{j}} \\ \boldsymbol{J} = \sigma \boldsymbol{E} + \boldsymbol{J}_{\mathrm{e}} \\ \boldsymbol{E} = -\nabla V \end{cases}, \tag{3}$$

where: $\boldsymbol{J}$ is the total current density, in A/m$^2$; $Q_{\mathrm{j}}$ is the charge quantity, in C; $\sigma$ is the conductivity, in S/m; $\boldsymbol{J}_{\mathrm{e}}$ is the external current density, in A/m$^2$.

#### 2.1.3. Particle field governing equation

The deposition of contaminant particles on the surface of an insulator is greatly affected by electric field force, fluid drag force and gravity, while other small forces, such as Van der Waals force, can be ignored [15]. The particle motion governing equation is shown in Formula (4) [16]:

$$m_{\mathrm{p}} \frac{\mathrm{d}\boldsymbol{v}}{\mathrm{d}t} = \boldsymbol{F}_{\mathrm{t}}, \tag{4}$$

where: $m_{\mathrm{p}}$ is the mass of the particle, in kg; $\boldsymbol{v}$ is the velocity of the particle, in m/s; $\boldsymbol{F}_{\mathrm{t}}$ is the total force acting on the particle, in N.

### 2.2. Measurement criteria for polluted insulators

The Non-Soluble Deposit Density (NSDD) is used to characterize the contamination level of per unit surface area of the insulator, in mg/cm$^2$. The calculation of NSDD values in the wind tunnel experiment and simulation are shown in Formulas (5) and (6), respectively.

$$\mathrm{NSDD} = \xi \frac{n m_{\mathrm{p}} t_{\mathrm{s}}}{t_{\mathrm{p}} S_{\mathrm{A}}}, \tag{5}$$

$$\mathrm{NSDD} = \frac{m_{\mathrm{e}}}{S_{\mathrm{A}}}, \tag{6}$$

where: $\xi$ is the time coefficient; $n$ is the total number of deposited pollutant particles on the simulated shed surface; $t_{\mathrm{p}}$ is the duration of simulated contaminant deposition in seconds, in s; $t_{\mathrm{s}}$ is the duration of contaminant deposition in the wind tunnel experiment, in s; $S_{\mathrm{A}}$ is the total surface area of the insulator shed, in m$^2$; $m_{\mathrm{e}}$ is the total mass of pollutants on the shed surface in the wind tunnel experiment, in kg.

### 2.3. Rationality verification

In this section, the validity of the simulation model and method is established through experiments conducted on the FXBW-330/120 insulator. Artificial contamination tests were performed at the wind tunnel laboratory at North China Electric Power University [17]. Due to the height restraint of the laboratory's wind tunnel, five sets of sheds of the FXBW-330/120 insulator were selected for contamination testing in the low-speed section of the wind tunnel, while DC voltages of (±18, ±24, ±30, ±36) kV were applied. In the experiment, the wind speed was set to 4 m/s. The polluted sample was prepared by mixing fine sand particles with an approximate particle size of 100 µm, diatomaceous earth particles with an approximate particle size of 50 µm, and NaCl

particles with an approximate particle size of 100 μm. The mixing ratio of these components was 6:6:1. Due to the larger particle size of fine sand and NaCl, they were not easily blown away at a wind speed of 4 m/s. On the other hand, the smaller particle size of diatomaceous earth made it more likely to be blown away. Therefore, the main pollutant component in the wind tunnel was diatomaceous earth. During the experiment, the overall contamination concentration was relatively low due to the low wind speed. Measurements showed that the concentration inside the wind tunnel was 0.256 mg/m$^3$, which is considered to be a relatively low concentration and can be regarded as being in line with the contaminant content in the air under natural conditions.

In COMSOL, a 3D computational domain with the same dimensions as the experimental section was established based on the parameters provided by the manufacturer, as shown in Fig. 1. The dimensions of the computational domain were set to 10.5 m × 1.1 m × 0.8 m in order to make the model closer to the conditions in the real environment, and a 100 mm thick infinite meta-domain was added around the computational domain to simulate an infinite space, as shown in Fig. 1. In Fig. 1, the left and right sides of the simulation domain were designated as the wind inlet and outlet, respectively, and the wind speed was set to 4 m/s. The flow medium in the domain was set as air, with a density of 1.29 kg/m$^3$ and a dynamic viscosity of $1.79 \times 10^{-6}$ Pa·s, and the insulator sheds material was set to silicone rubber, with a relative permittivity of 3.0, a relative permeability of 1, and a volume resistivity of $1.0 \times 10^{15}$ Ω·cm. The mandrel material was set as a glass fiber reinforced epoxy resin material, with a relative dielectric coefficient of 2.0, and a volume resistivity of $3.0 \times 10^{15}$ Ω·cm; The fittings were set as an aluminum alloy material, and their conductivity was set to $3.5 \times 10^7$ S/m, which was in line with the physical properties of the actual material. Contaminant particles were released from the inlet, and the particle charge was set as the fly ash charge [18], where 31% of particles had an average charge-to-mass ratio of $+6.3 \times 10^{-3}$ C/kg, 26% of particles had an average charge-to-mass ratio of $-7.0 \times 10^{-3}$ C/kg, and 43% of particles were neutral. The particle deposition criterion [12] was applied to the insulator surface, and if the deposition criterion was met, particles would be deposited on the surface of the insulator, otherwise diffused reflection would occur. The particle deposition criterion is shown in Formula (7):

$$\begin{cases} r + F_{\mathrm{w}} l_{\mathrm{w}} + E_{\mathrm{p}} \cos^2\theta + F_{\mathrm{g}} l_{\mathrm{g}} \cos\theta - \left(F_{\mathrm{p}} l_{\mathrm{p}} + E_{\mathrm{s}} E_{\theta} q l_{\mathrm{e}}\right) \geq 0 \\ q E_{\mathrm{s}} \overrightarrow{E_{\mathrm{tx}}} \cdot \overrightarrow{l_{\mathrm{f}}} + E_{\mathrm{p}} \sin^2\theta \cos^2\varphi \leq F_{\mathrm{f}} l_{\mathrm{f}} \\ q E_{\mathrm{s}} \overrightarrow{E_{\mathrm{ty}}} \cdot \overrightarrow{l_{\mathrm{f}}} + E_{\mathrm{p}} \sin^2\theta \sin^2\varphi \leq F_{\mathrm{f}} l_{\mathrm{f}} \end{cases}, \tag{7}$$

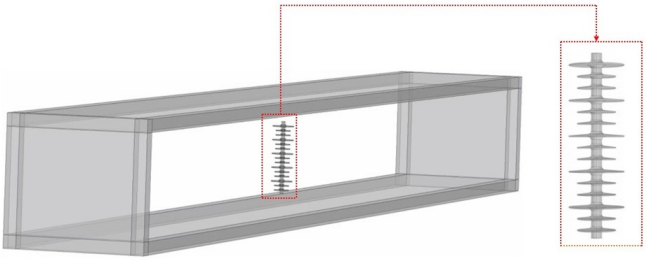

Fig. 1. Contaminant deposition simulation domain of FXBW-330/120 insulator

where: $l_w$, $l_p$, $l_f$, $l_g$, and $l_e$ are the corresponding action distances of each force (each action distance is short and has a limited range, so the value is initialized accordingly), in m; $E_p$ is the kinetic energy of the particle before collision, in J; $\theta$ is in the earth coordinate system, the $\theta$ is coordinates of the collision points; $\varphi$ is in the earth coordinate system, the $\varphi$ is coordinates of the collision points; $E_s$ is the modulus of the electric field vector at the collision point, in V/m; $E_{tx}$ and $E_{ty}$ are the $x$- and $y$-components, respectively, of the unit vector of the electric field strength at the collision point. $r$ is the effect of the surface energy, and $r = A\sqrt{r_1 r_2}$ ($r_1$ and $r_2$ are the surface energies of the pollution particles and insulator sheds, respectively), in J/m$^2$; $A$ is the projected area of the particle on the surface of the insulator, in m$^2$.

Table 1 compares the experimental and simulation NSDD results, revealing a certain error between them, with an average relative error of 15.54%, which falls within the acceptable range for engineering applications. The error may be attributed to the difference between the particle charge quantity used in the wind tunnel experiment and the fly ash charge used in the simulation model. Additionally, in the measurement of the contamination level on the insulator surface, there is often some residual contamination, which may also contribute to the error. Given these factors, the simulation results presented in this paper are deemed to be more reasonable under ideal conditions.

Table 1. NSDD comparison between wind tunnel experiment and simulation

| **Parameter** | **Value** | | | | | | | | **Unit** |
|---|---|---|---|---|---|---|---|---|---|
| Voltage | –36 | +36 | –30 | +30 | –24 | +24 | –18 | +18 | kV |
| Experiment | 0.35 | 0.40 | 0.30 | 0.34 | 0.26 | 0.33 | 0.21 | 0.24 | mg/cm$^2$ |
| Simulation | 0.34 | 0.49 | 0.33 | 0.39 | 0.32 | 0.34 | 0.26 | 0.30 | mg/cm$^2$ |

## 3. Numerical simulation research on structural optimization of insulators

### 3.1. Structural parameters of insulators

In power transmission systems, large and small alternating shed insulators are widely used in all regions due to their comprehensive antifouling and flashover performance. Therefore, this section takes the FXBW4-110/100 insulator as an example and uses the numerical simulation method to explore the effects of shed inclination angles $\alpha$ and $\beta$, and shed spacing $s$ on its antifouling performance. Table 2 lists its main structural parameters, and Fig. 2 shows a schematic diagram of the insulator structure.

In order to investigate the impacts of the shed spacing $s$, and shed inclination angles $\alpha$ and $\beta$ on the contamination characteristics of insulators, and facilitate the further exploration of these characteristics, a progressive structural optimization approach is applied to the simulation research in this paper. Literatures [19, 20] indicate that the typical ranges of the upper inclination angle $\alpha$ for AC and DC systems are 5°–25° and 0°–25°, respectively, while the lower inclination angle $\beta$ is smaller than the upper inclination angle $\alpha$. Additionally, based on long-term operational

Table 2. Main structural parameters of the FXBW4-110/100 insulator

| Parameter | Symbol | Value | Unit |
|---|---|---|---|
| Shed spacing | $s$ | 80 | mm |
| Upper inclination angle | $\alpha$ | 10 | ° |
| Lower inclination angle | $\beta$ | 2 | ° |
| Diameter of large shed | $D_2$ | 140 | mm |
| Diameter of small shed | $D_1$ | 112 | mm |

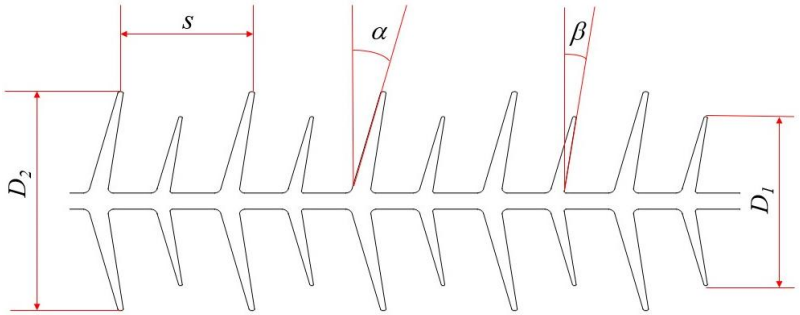


Fig. 2. Schematic diagram of insulator structure

experience of numerous transmission lines in China, literatures [21, 22] suggest that the typical range of the upper inclination angle $\alpha$ for AC and DC systems are 5°–15° and 1°–25°, respectively. An excessive lower inclination angle $\beta$ may cause the shed to become thinner, resulting in a decrease in the mechanical strength of the insulator. Meanwhile, a large shed spacing $s$ can increase the height of the insulator structure, resulting in difficult design of transmission line towers and other problems. Therefore, the shed spacing $s$ (80 mm–98 mm), upper inclination angle $\alpha$ under AC voltages (6°–14°), upper inclination angle $\alpha$ under DC voltages (2°–16°), and lower inclination angle $\beta$ (0°–6°) are selected as the variables for this study.

### 3.2. Single valuedness condition settings

In COMSOL, a contaminant deposition simulation domain of 2.0 m × 1.2 m × 2.0 m was established. A 100 mm thick infinite meta-domain was constructed around it to simulate the infinite air domain surrounding the insulator, as shown in Fig. 3. According to literatures [23, 24], a wind speed of 2.5 m/s, a particle size was defined as 20 μm and a density of 2 200 kg/m$^3$ are defined as typical conditions, and selected for simulated calculation. In simulated calculation, the upper end of the insulator was grounded, while AC/DC voltages of 110 kV were applied to the lower end, respectively. The material parameters and other boundary conditions are consistent with those in Section 2.3 and are not repeated here.

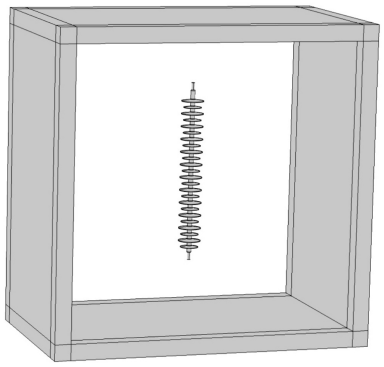

Fig. 3. Simulation domain for contaminant deposition of FXBW4-110/100 insulator

### 3.3. Progressive structural optimization scheme and simulation analysis for insulators

#### 3.3.1. Impact of shed spacing *s*

In this test the upper inclination angle $\alpha$ was kept at 10° and the lower inclination angle $\beta$ was kept at 2°, while changing the shed spacing $s$. Figure 4 shows the variation of the contaminant deposition of the insulator under DC and AC voltages with the shed spacing $s$. In Fig. 4, the horizontal axis represents the shed spacing $s$ (mm), and the vertical axis represents NSDD (mg/cm$^2$). As can be seen from Fig. 4, with the increase of the shed spacing $s$, the contaminant deposition of the insulator under both AC and DC voltages shows a downtrend.

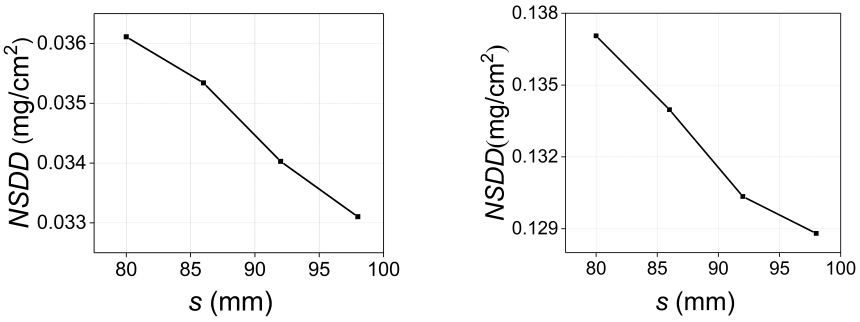


Fig. 4. Variation of contaminant deposition of insulator with shed spacing ***s*** under DC and AC voltages: (a) AC voltage; (b) DC voltage

Figure 5 shows the velocity streamline diagram of different shed spacings s when the upper inclination angle $\alpha$ was kept at 10° and the lower inclination angle $\beta$ was kept at 2°. The diagram reveals two effects of the shed spacing $s$ on the flow field characteristics surrounding the insulator. First, a larger shed spacing $s$ increases the range of the fluid vortex between the sheds of the insulator. This results in more polluted particles being entrained into the fluid vortex, thus increasing the likelihood of collision with the surface of the insulator. Second, a larger shed

spacing $s$ weakens the mutual interference between the flow fields of the sheds, reducing the strength of the fluid vortex and the residence time of polluted particles moving with the drag force. This results in reduced probability of collision between particles and the insulator. In this study, the contaminant deposition of the insulator decreases as the shed spacing $s$ increases. This result may be attributed to the stronger mutual interference between the flow fields of the sheds of the insulator compared to the effect of the fluid vortex area between the sheds. Therefore, within the scope (80 mm $\leq$ s $\leq$ 98 mm) of this study, a shed spacing $s$ of 98 mm has the best antifouling effect.

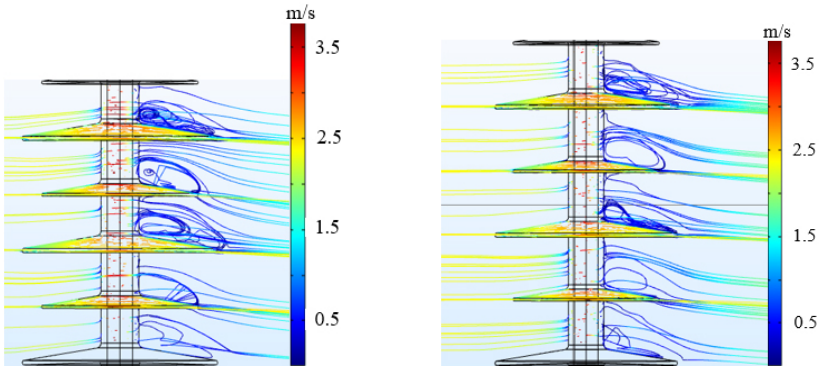


(a) (b)

Fig. 5. Velocity streamlines at different shed spacings $s$: (a) $s$ = 80 mm; (b) $s$ = 98 mm

### 3.3.2. Impact of upper inclination angle $\alpha$

In this test the shed spacing $s$ was kept at 98 mm and the lower inclination angle $\beta$ was kept at 2°, while changing the upper inclination angle $\alpha$. Figure 6 shows the variation of contaminant deposition of the insulator under DC and AC voltages with the upper inclination angle $\alpha$. In Fig. 6, the horizontal axis represents the upper inclination angle $\alpha$ (°), and the vertical axis represents NSDD (mg/cm$^2$). From Fig. 6(a), it can be observed that the contaminant deposition of the insulator under AC voltages increases with the upper inclination angle $\alpha$, which is consistent with the research results on the variation of the contaminant deposition of insulators in AC systems with the upper inclination angle $\alpha$ in literature [19]. This also indirectly confirms the rationality of the contaminant deposition model proposed in this paper. From Fig. 6(b), it can be seen that with the increase of the upper inclination angle $\alpha$, the contaminant deposition of the insulator under DC voltages exhibits a skewed $N$-shaped variation trend, initially rising, then declining and then rising again.

Figure 7 shows the velocity streamline diagram of different upper inclination angles $\alpha$ when the shed spacing of the insulator $s$ was kept at 98 mm and the lower inclination angle $\beta$ was kept at 2°. It can be seen from Fig. 7 that the upper inclination angles $\alpha$ of the insulator will have two effects on the flow field: With the increase of the upper inclination angle $\alpha$, on the one hand, the upper surface of the insulator will collide with more incoming particles, increasing the probability of particle deposition; on the other hand, the fluid vortex scale on the leeward side of

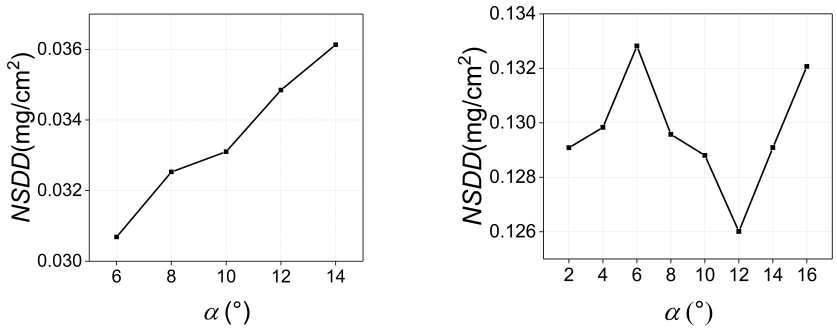


Fig. 6. Variation of contaminant deposition of the insulator with upper inclination angle $\alpha$ under DC and AC voltages: (a) AC voltage; (b) DC voltage

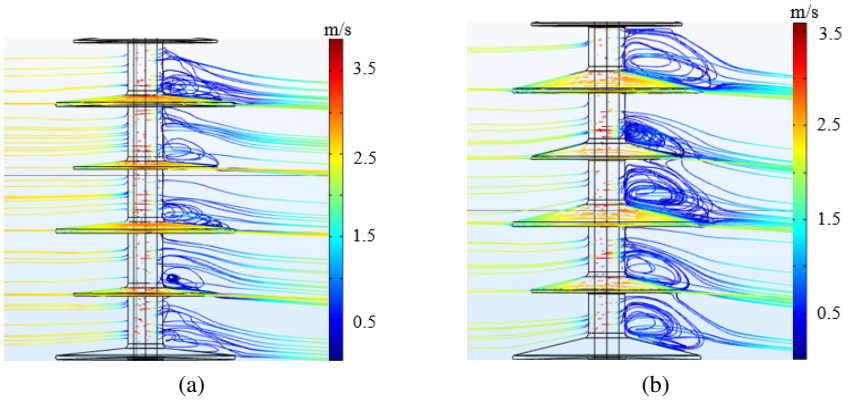


Fig. 7. Velocity streamlines at different upper inclination angles $\alpha$: (a) $\alpha = 6°$; (b) $\alpha = 14°$

the insulator will increase, and the number of vortices generated will also increase significantly, making particles more likely to deposit on its surface. Within the scope of this study, under AC voltages, the contaminant deposition of the insulator increases with the upper inclination angle $\alpha$, possibly because under AC voltages, the direction of the electric field force of charged particles changes periodically with time. When the AC electric field and the flow field jointly affect the deposition behavior of particles, the effect of the flow field on the deposition behavior of particles becomes dominant. However, under DC voltages, the contaminant deposition of the insulator shows an uptrend first, then a downtrend and then an uptrend again with the increase of the upper inclination angle $\alpha$, possibly because under DC voltages, the direction of the electric field force of charged particles is constant, and the effect of the DC electric field on particle deposition is stronger than that of the AC electric field. When the upper inclination angle $\alpha$ of the insulator increases, the directed tangential electric field force applied on charged particles on the upper surface of the insulator increases, so that some charged particles leave its surface. Therefore,

within the scope of this study, the optimal upper inclination angle $\alpha$ for insulator contamination prevention under AC voltages is 6°, while under DC voltages, the optimal upper inclination angle $\alpha$ is 12°.

#### 3.3.3. Impact of lower inclination angle $\beta$

In this test the shed spacing $s$ of the insulator was kept at 98 mm and the upper inclination angle $\alpha$ was kept at 6° under AC voltages, and the shed spacing $s$ was kept at 98 mm and the upper inclination angle $\alpha$ was kept at 12° under DC voltages, while changing the lower inclination angle $\beta$ of the insulator. Figure 8 shows the variation of the contaminant deposition of the insulator under DC and AC voltages at different lower inclination angles $\beta$. In Fig. 8, the horizontal axis represents the lower inclination angle $\beta$ (°), and the vertical axis represents NSDD (mg/cm$^2$). It can be seen from Fig. 8 that with the increase of the lower inclination angle $\beta$ of the insulator, its contaminant deposition shows an uptrend.

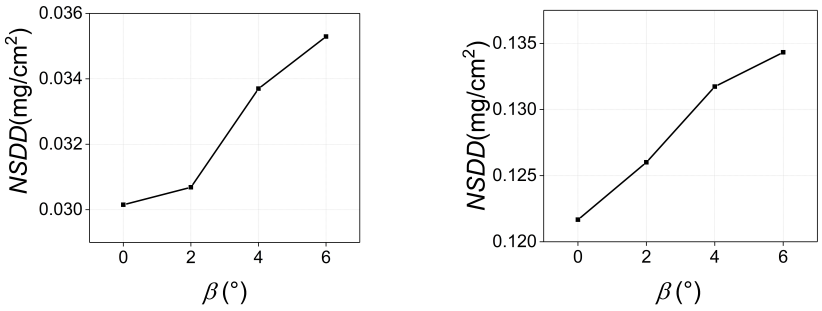


Fig. 8. Variation of insulator contamination with the lower inclination angle $\beta$ under DC and AC voltages: (a) AC voltage; (b) DC voltage

Figure 9 shows the velocity streamline diagrams at different lower inclination angles $\beta$ of the insulator with a shed spacing $s$ was kept at 98 mm and an upper inclination angle $\alpha$ was kept at 6°. As shown in Fig. 9(a), when the lower inclination angle $\beta$ is 0°, the flow lines near the underside of the shed surface of the insulator are relatively straight, with few bends, and vortices are mainly generated near the upper surface of the shed. As shown in Fig. 9(b), when the lower inclination angle $\beta$ increases to 6°, the flow lines near the underside of the insulator shed surface bend greatly and the fluid vortex scale increases. Within the scope of this study, the contaminant deposition on the insulator increases with the lower inclination angle $\beta$, possibly because the fluid vortex scale between the sheds increases with the lower inclination angle $\beta$, resulting in more particle deposition on the shed surface. Therefore, within the scope of this study, the optimal lower inclination angle $\beta$ for contamination prevention is 0°.

Insulators usually operate in multiple environments, and a smaller lower inclination angle $\beta$ is not conducive to the flow of rainwater. Considering the practical needs of engineering applications, this paper optimizes the structure of the insulator. The optimized model has an upper inclination angle $\alpha$ is kept at 6°, a lower inclination angle $\beta$ is kept at 2°, and a shed spacing $s$ is kept at 98 mm, and is referred to as the AC-optimized model for convenience.

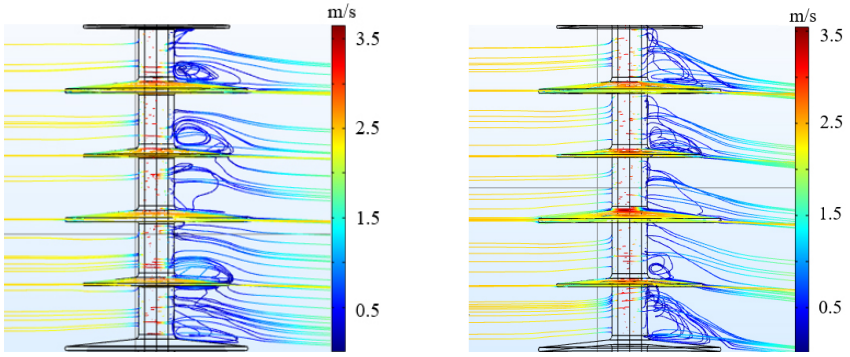


(a) (b)

Fig. 9. Velocity streamlines at different lower inclination angles $\beta$: $\beta = 0°$; (b) $\beta = 6°$

### 3.4. Comparative analysis of contaminant deposition of insulators under AC voltages

#### 3.4.1. Comparison of contaminant depositions at different wind speeds

When the concentration of contaminant particles in the air is 0.3 mg/m$^3$ and the particle density is 2 200 kg$^3$, Fig. 10 shows the comparison of contaminant depositions of the insulator before and after optimization at different wind speeds under AC voltages. In Fig. 10, the horizontal axis represents the wind speed (m/s), and the vertical axis represents NSDD (mg/cm$^2$). As shown in Fig. 10, the contaminant deposition on the insulators increases with wind speed. Under the working conditions of 2, 3, 4 and 5 (m/s), the AC-optimized model demonstrates better contamination resistance compared to the original model. At wind speeds of 2, 3, 4 and 5 (m/s), respectively, the contaminant depositions of the AC-optimized model are 77.4%~90.4% of those of the original model (77.4% at a particle size of 20 μm and 90.4% at 15 μm), 81.0%~90.3% (81.0% at a particle size of 25 μm and 90.3% at 15 μm), 82.7%~89.5% (82.7% at a particle size of 25 μm and 89.5% at 15 μm), 87.7%~92.7% (87.7% at a particle size of 20 μm and 92.7% at 15 μm), averaging 85.2%, 86.5%, 86.1% and 90.5% of the original model, respectively.

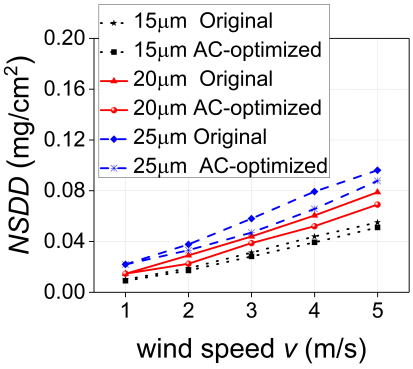


Fig. 10. Impacts of different wind speeds on contaminant deposition under AC voltages

However, at a wind speed of 1 m/s, there is a relatively small difference in contaminant deposition between the two types of insulators, and in some cases, the AC-optimized model even shows higher contaminant deposition than the original model for certain particle sizes (20 μm), possibly because on the one hand, the increased shed spacing $s$ creates a large-scale, low-speed vortex area that favors particle deposition, and on the other hand, at low wind speeds, the impact of gravity on particles increases relative to the drag force, and the impact of the flow field on the contaminant deposition of insulators is weakened.

#### 3.4.2. Comparison of contaminant depositions at different particle sizes

When the concentration of contaminant particles in the air is 0.3 mg/m$^3$ and the particle density is 2 200 kg$^3$, Fig. 11 shows the comparison of contaminant depositions of the insulator before and after optimization at different particle sizes under AC voltages at wind speeds of 2, 3 and 4 m/s, respectively. In Fig. 11, the $x$-axis represents the particle size (μm), and the $y$-axis represents NSDD (mg/cm$^2$). It can be seen from Fig. 11 that the contaminant deposition of the insulator increases with particle size.

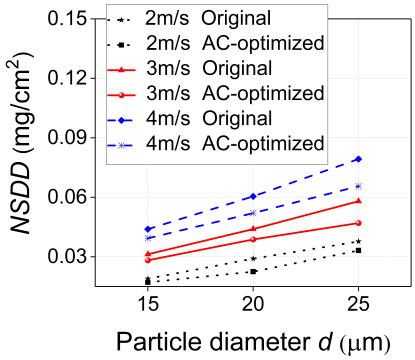


Fig. 11. Impacts of different particle sizes on contaminant deposition under AC voltages

In addition, under the conditions in Section 3.4.2, the AC-optimized model shows significantly better contamination mitigation characteristics than the original model. At particle sizes of 15, 20 and 25 μm, the contaminant depositions of the AC-optimized model are 89.5%~90.4% of those of the original model (89.5% at a wind speed of 4 m/s and 90.4% at 2 m/s), 77.4%~88.2% (77.4% at a wind speed of 2 m/s and 88.2% at 3 m/s), and 81.0%~87.9% (81.0% at a wind speed of 3 m/s and 87.9% at 2 m/s), respectively. On average, the AC-optimized model performs at 90.0%, 85.9% and 85.9% of the original model, respectively.

#### 3.4.3. Comparison of contaminant depositions at different particle densities

When the concentration of contaminant particles in the air is 0.3 mg/m$^3$, Fig. 12 shows the comparison of contaminant depositions of the insulator before and after optimization at different particle densities under AC voltages. In Fig. 12, the $x$-axis represents the particle density (kg/m$^3$), and the $y$-axis represents NSDD (mg/cm$^2$). From the five sub-figures in Fig. 12, it can be seen that overall, the contaminant deposition of the insulator increases with particle density.

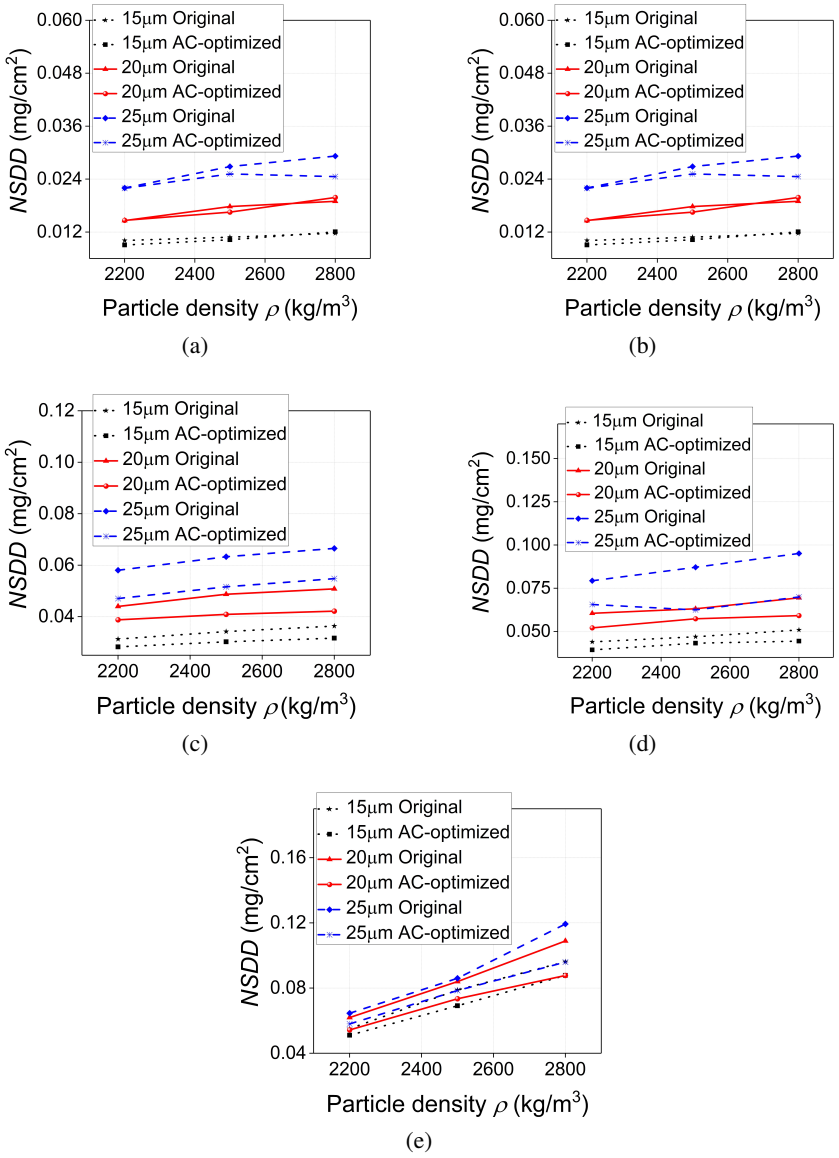


Fig. 12. Impacts of particle density on contaminant deposition at different wind speeds under AC voltages: (a) $v$ = 1 m/s; (b) $v$ = 2 m/s; (c) $v$ = 3 m/s; (d) $v$ = 4 m/s; (e) $v$ = 5 m/s

At a wind speed of 1 m/s, at three different densities, the AC-optimized model performs the worst in terms of contamination mitigation. For example, at a particle density of 2 800 kg/m$^3$ and a particle size of 15 μm, the contaminant deposition of the AC-optimized model is 0.0121 mg/cm$^2$, while for the original model, it is 0.0117 mg/cm$^2$, indicating the deterioration of the AC-optimized model in in contaminant deposition.

However, at ambient wind speeds of 2–5 m/s, and particle densities of 2 200, 2 500 and 2 800 kg$^3$ respectively, the contaminant depositions of the AC-optimized model are 77.4%~92.7% of the original model (77.4% at a wind speed of 2 m/s and a particle size of 20 μm, and 92.7% at a wind speed of 4 m/s and a particle size of 20 μm), 71.7%~92.7% (71.7% at a wind speed of 4 m/s and a particle size of 25 μm, and 92.7% at a wind speed of 4 m/s and a particle size of 15 μm), and 73.5%~91.9% (73.5% at a wind speed of 4 m/s and a particle size of 25 μm, and 91.9% at a wind speed of 5 m/s and a particle size of 20 μm). On average, the AC-optimized model performs at 87.1%, 84.3% and 84.2% of the original model, respectively.

This indicates that when the wind speed is greater than 1 m/s, the AC-optimized model still exhibits superior contamination mitigation performance in a wide range of environmental conditions with broad particle sizes (15–25 μm) and high particle densities (2 200–2 800 kg/m$^3$). Its application potential and prospects are considerable.

Based on these results, it is advised to appropriately reduce the shed inclination angles $\alpha$ and $\beta$, and increase the shed spacing $s$ when designing and manufacturing insulators for AC systems in areas with higher average wind speeds ($\geq$ 2 m/s) to improve their antifouling performance.

## 4. Conclusion

1. With the increase of the shed spacing $s$, the strength of fluid vortices among shed decreases, and the amount of insulator contaminant deposition decreases under both AC and DC voltages.
2. The amount of insulator contaminant deposition under the action of AC voltages increases with the increase of the upper inclination angle $\alpha$, but under DC voltages, due to the impact of directional electric field forces, the amount of contaminant deposition shows a change trend of "$N$"; under AC/DC voltages, the amount of contaminant deposition increases with the increase of the low inclination angle $\beta$, and under AC voltages, the amount of contaminant deposition is more likely to be affected by the low inclination angle. The optimal upper inclination angles $\alpha$ of the insulator under AC/DC voltages are 6° and 12°, respectively, and the optimal low inclination angle $\beta$ is 0°.
3. The AC-optimized model shows superior antifouling performance in environments with $v \geq$ 2 m/s, and under the typical conditions ($v$ = 2.5 m/s, $d$ = 20 μm, $\rho$ = 2 200 kg/m$^3$), the amount of contaminant deposition of the AC-optimized model is reduced by 15.0% compared with the original model. It is recommended that insulators with smaller shed inclination angles and larger shed spacings be used in 110 kV AC transmission lines in areas with an average wind speed of not less than 2 m/s.
4. In this paper, a study on the structural optimization of insulators is carried out under common working conditions in China. However, due to regional differences in environmental conditions, in some low wind speed areas ($v$ < 2 m/s), the impact of particle settlement on insulator contaminant deposition cannot be ignored. In the future, the impact of insulator structure on particle settlement at low wind speeds can be explored, which can provide a reference for insulator structural design in different environments.

**References**


[1] Lan L., Mu L., Wang Y., Yuan X.Q., Wang W., Li Z. H., *The influence of pollution accumulation on coating aging of UHV line insulators with different suspension height in coal ash polluted area*, Archives of Electrical Engineering, vol. 69, no. 1, pp. 39–56 (2020), DOI: 10.24425/aee.2020.131757.

[2] Bychkov P.N., Zabrodina I.K., Shlapak V.S., *Insulation contamination of overhead transmission lines by extreme service conditions*, IEEE Transactions on Dielectrics and Electrical Insulation, vol. 23, no. 1, pp. 288–293 (2016), DOI: 10.1109/TDEI.2015.005323.

[3] Yang L.G., Pauli F., Zhang S.M., Hambrecht F., Hameyer K., *Influence of conductive particle contamination on the insulation system of rotating electrical machines with direct oil cooling*, Archives of Electrical Engineering, vol. 71, no. 3, pp. 789–804 (2022), DOI: 10.24425/aee.2022.141 685.

[4] El-hag A.H., Jayaram S.H., Cherney E.A., *Effect of insulator profile on aging performance of silicone rubber insulators in salt-fog*, IEEE Transactions on Dielectrics and Electrical Insulation, vol. 14, no. 2, pp. 352–359 (2007), DOI: 10.1109/TDEI.2007.344615.

[5] Gafti A., Taherian R., Kiahoseini S.R., *Chemical composition optimization of nanocomposites used for shed and core of outdoor composite insulators*, Frontiers in Materials, vol. 9 (2022), DOI: 10.3389/fmats.2022.1024730.

[6] Li L.C., Gu Y., Hao Y.P., Xue Y.W., Xiong G.K., Yang L., Zhang F.Z., *Shed Parameters Optimization of Composite Post Insulators for UHV DC Flashover Voltages at High Altitudes*, IEEE Transactions on Dielectrics and Electrical Insulation, vol. 22, no. 1, pp. 169–176 (2015), DOI: 10.1109/TDEI.2014.004528.

[7] You J.W., *Study on Contamination Characteristics of Typical Insulators Tested in Wind Tunnel*, Master Thesis, Chongqing University, Chongqing (2016).

[8] Liu Q., Xie L., Nan J., *External Insulation Characteristics and Anti-ice Umbrella Application of HV Composite Post Insulator*, High Voltage Engineering, vol. 46, no. 8, pp. 2872–2879 (2020).

[9] Madi A.M., He Y.D., Jiang L.L., *Design and testing of an improved profile for silicone rubber composite insulators*, IEEE Transactions on Dielectrics and Electrical Insulation, vol. 24, no. 5, pp. 2930–2936 (2017), DOI: 10.1109/TDEI.2017.006170.

[10] Mariprasath T., Asokan S., Ravindaran M., *Comparison and Optimization of Various Coated Ceramic Insulator Artificial Coastal Thermal Power Plant Pollution*, Journal of Circuits Systems and Computers, vol. 29, no. 12 (2020), DOI: 10.1142/S0218126620501996.

[11] El-Refaie E.M., Abd Elrahman M.K., Mohamed M.K., *Electric field distribution of optimized composite insulator profiles under different pollution conditions*, Ain Shams Engineering Journal, vol. 9, no. 4, pp. 1349–1356 (2018), DOI: 10.1016/j.asej.2016.08.012.

[12] Lv Y.K., Zhao W.P., Yan W.P., Liu Y.P., *Optimization of the contamination particle deposition model based on humidity and surface energy*, Applied Thermal Engineering, vol. 157, no. 11, article 113734 (2019), DOI: 10.1016/j.applthermaleng.2019.113734.

[13] Lv Y.K., Chen Z.Z., Ge Q.Z., Wang Q., Zhang Y.Z., *Numerical Simulation of Contamination Accumulation Characteristics of Composite Insulators in Salt Fog Environment*, Energy Engineering: Journal of the Association of Energy Engineering, vol. 120, no. 2, pp. 483–499 (2023), DOI: 10.32604/ee.2023.023649.

[14] Wang G.Z., Chen Q., *Simulation on Contamination Depositing Characteristics of Electrified Railway Catenary Insulators*, Insulators, and Surge Arresters, vol. 298, no. 6, pp. 228–234+240 (2020).

[15] Li M.Z., Mei H.W., Cheng D.F., Xia L.Z., Cao B., Wang L.M., *Influence of Electric Field on Contamination Accumulation Characteristics of Glass Material*, High Voltage Engineering, vol. 47, no. 10, pp. 3581–3589 (2021).

[16] Huang Z.C., Liu Y.P., Geng J.H., Li H., Kong Y.X., Liu J.X., *Model and Experimental Verification of Particle Collision Capture on Composite Insulator Surface*, High Voltage Engineering, vol. 48, no. 3, pp. 902–913 (2022).

[17] Lv F.C., Huang H., Liu Y.P., Qin C.X., Liu Q., Xu T., *Contamination Depositing Characteristics of Insulators Under Natural Crosswind Conditions with Wind Tunnel Simulation*, High Voltage Engineering, vol. 40, no. 5, pp. 1281–1289 (2014).

[18] White H.J., *Industrial electrostatic precipitator*, Reading UK: Addison-Wesley (1963).

[19] IEC TS 60815, *Selection and dimensioning of high-voltage insulators intended for use in polluted conditions – Part 3: Polymer insulators for a.c. systems* (2008).

[20] IEC TS 60815, *Selection and dimensioning of high-voltage insulators intended for use in polluted conditions – Part 4: Insulators for d.c. systems* (2016).

[21] GB/T 26218, *Selection and dimensioning of high-voltage insulators intended for use in polluted conditions – Part 3: Composite insulators for a.c. systems* (2011).

[22] GB/T 26218, *Selection and dimensioning of high-voltage insulators intended for use in polluted conditions – Part 4: Insulators for d.c. systems* (2019).

[23] Wang N., *Long-term Trend of Surface Wind Speed and Wind Energy over China in Recent 36 Years*, Journal of Natural Resources, Master Thesis, Nanjing University of Information Science and Technology, Nanjing (2019).

[24] Jiang M., Jiang Y.P., Lu M., Li L., *Study on Particle Size Distribution and Mechanism of Natural Contaminated Particles on the Surface of Composite Insulator*, High Voltage Apparatus, vol. 57, no. 12, pp. 17–24 (2021).